



## 1 Remote Quantification of the Trophic Status of Chinese Lakes

2 Sijia Li<sup>a</sup>, Shiqi Xu<sup>a</sup>, Kaishan Song<sup>a</sup>, Tiit Kutser<sup>b</sup>, Zhidan Wen<sup>a\*</sup>, Ge Liu<sup>a</sup>, Yingxin Shang<sup>a</sup>,

3 Lili Lyu<sup>a</sup>, Hui Tao<sup>a</sup>, Xiang Wang<sup>a</sup>, Lele Zhang<sup>a</sup>, Fangfang Chen<sup>a</sup>

4 <sup>a</sup> Northeast Institute of Geography and Agroecology, Chinese Academy of Sciences, Changchun  
5 130102, China. P. R

6 <sup>b</sup> Estonian Marine Institute, University of Tartu, Mäealuse 14, 12618 Tallinn, Estonia

7

8 Correspondence to: Zhidan Wen ([wenzhidan@iga.ac.cn](mailto:wenzhidan@iga.ac.cn))

9 **Abstract:** Assessing eutrophication in lakes is of key importance, as this parameter  
10 constitutes a major aquatic ecosystem integrity indicator. The trophic state index (*TSI*),  
11 which is widely used to quantify eutrophication, is a universal paradigm in scientific  
12 literature. In this study, a methodological framework is proposed for quantifying and  
13 mapping *TSI* using the Sentinel Multispectral Imager sensor and fieldwork samples. The  
14 first step of the methodology involves the implementation of stepwise multiple  
15 regression analysis of the available *TSI* dataset to find some band ratios, such as  
16 blue/red, green/red, and red/red, which are sensitive to lake *TSI*. Trained with in situ  
17 measured *TSI* and match-up Sentinel images, we established the XGBoost of machine  
18 learning approaches to estimate *TSI*, with good agreement ( $R^2=0.87$ , slope=0.85) and  
19 fewer errors (MAE= 3.15 and RMSE=4.11). Additionally, we discussed the  
20 transferability and applications of XGBoost in three lake classifications: water quality,  
21 absorption contribution, and reflectance spectra types. We selected the XGBoost to map  
22 *TSI* in 2019-2020 with good quality Sentinel-2 Level-1C images embedded in ESA to  
23 examine the spatiotemporal variations of the lake trophic state. In a large-scale  
24 observation, 10-m *TSI* products from investigated 555 lakes in China facing  
25 eutrophication and unbalanced spatial patterns associated with lake basin characteristics,  
26 climate, and anthropogenic activities. The methodological framework proposed herein  
27 could serve as a useful resource toward a continuous, long-term, and large-scale



28 monitoring of lake aquatic ecosystems, supporting sustainable water resource  
29 management.

## 30 **1 Introduction**

31 Lakes, as valid sentinels of global or regional responses, are sensitive to  
32 anthropogenic activities and climate change (Mortsch et al., 1996; Quayle et al., 2002;  
33 Tranvik et al., 2009). The commonly used paradigm for studying eco-environmental  
34 monitoring and controlling of lakes is the status of eutrophication (Carlson, 1977). It is  
35 a combination of light, heat, hydrodynamics, and nutrients, such as nitrogen and  
36 phosphorus, which occurs through a series of biological, chemical, and physical  
37 processes of lakes. As a result of eutrophication, nutrient loading and productivity grow  
38 sharply, and even hypoxia and frequent outbreaks of harmful algal blooms are likely to  
39 produce toxins (Paerl et al., 2008, 2011). These processes can cause serious degradation  
40 of water quality and are detrimental to the ecosystem services functionality of lakes and  
41 reliable supply of drinking water (OECD, 1982). Once the eutrophication phenomenon  
42 becomes intense, ecological imbalances generally follow (Smith et al., 2006). Hence,  
43 knowledge of the process of eutrophication can provide us with an understanding of the  
44 structure and function of lake ecosystems that give rise to environmental changes. We  
45 can then predict future trends and develop appropriate mitigation strategies.

46 Several lakes experience eutrophication processes because of excessive nutrient  
47 enrichment (Lund, 1967; Smith et al., 1999; Wetzel, 2001). At the global scale, 63.1%  
48 of lakes larger than 25 km<sup>2</sup> are eutrophic and 54% of Asian lakes (Wang et al., 2018), as  
49 well as 53% of European lakes (ILEC et al., 1994). Lake eutrophication has become a  
50 global water quality issue affecting most freshwater ecosystems (Matthews, 2014).  
51 Currently, many pollutions control measures and management strategies have been  
52 implemented that are specific to individual lakes or to lakes, in general (USEPA, 2002).



53 However, there is still insufficient information to address lake eutrophication related to  
54 environmental disturbances or changes. Realization of lake eutrophication has been a  
55 serious situation for some lakes; therefore, we provided some reasons to suggest the  
56 need for large-scale research. First, different environmental factors control the trophic  
57 status of lakes at local and multiple scales (e.g., Wiley et al., 1997). Specifically, biotic  
58 factors may dominate the eutrophic state of individual lakes, and we can understand the  
59 mechanism processes by lake-specific sampling. In contrast, abiotic factors and their  
60 linkages are pivotal factors that determine lake biogeochemistry at multiple scales (Sass  
61 et al., 2007). It is often necessary to study a number of lakes with different  
62 characteristics and catchments to understand the mechanisms of spatio-temporal  
63 patterns. Therefore, an up-scaling study of trophic status is required to understand the  
64 evolution prospects of lakes in response to changes in global and regional environments.  
65 Second, multi-year environmental and climatic conditions require long-term field  
66 studies and observations to understand the temporal pattern in important trophic status  
67 processes. In addition, relatively large datasets are needed considering the spatial extent  
68 because environmental factors are integrated to determine the trophic status of lakes. It  
69 can promote data organization and enable us to address an emergency and establish  
70 scientific measures for water resource management (Cunha et al., 2013; Smith and  
71 Schindler, 2009). Thus, eutrophication should be rapidly assessed using easy-to-analyze  
72 indices and enforcement methods for large-scale and high-frequency applications.

73 Evaluating the trophic state of lakes has been an important topic for decades  
74 (Carlson, 1977; Smith and Schindler 2009). The traditional method uses chlorophyll-a,  
75 transparency, nutrients, and other variables as water quality indicators by field in situ  
76 sampling and laboratory measurements (Rodhe, 1969). Subsequently, Carlson (1977)  
77 introduced a numerical *TSI* that should have replaced descriptive values like



78 “oligotrophic,” “mesotrophic,” or “eutrophic”. The replacement has not occurred, but  
79 the *TSI* proposed by Carlson is a common method to determine the trophic state level of  
80 aquatic environments (Aizaki et al., 1981). The traditional method for calculating *TSI* is  
81 based on collected in situ data. The sampling itself and subsequent laboratory  
82 measurements are labor-intensive and expensive, often also logistically difficult to  
83 perform. This limits our capability to monitor hundreds or thousands of lakes for  
84 eutrophication, not speaking about the majority of 117 million of lakes on Earth  
85 (Verpoorter et al. 2014). Moreover, the *TSI* calculated for one or a few discrete samples  
86 do not represent spatial distribution of *TSI* within (especially larger) lakes. This could  
87 limit the large-scale assessment of eutrophication as well as the understanding of  
88 biogeochemical cycles.

89         Satellite remote sensing is a useful tool for monitoring inland waters (Palmer et  
90 al 2015). Ocean water-color sensors, such as Medium Resolution Imaging Spectrometer  
91 (MERIS) or Ocean and Land Colour Instrument (OLCI) have too low spatial resolution  
92 (300 m) for majority of lakes on Earth. Land remote sensing sensor like Landsat  
93 Operational Land Imager (OLI), Sentinel-2 Multispectral Imager (MSI; 10-60 m) and  
94 Satellite pour l'Observation de la Terre (SPOT) with high spatial resolution (5–30 m) are  
95 not designed for water remote sensing (lack critical spectral bands, SNR is not sufficient  
96 for water, etc.). Compared to OLI and SPOT sensors, MSI has a more adequate  
97 radiometric resolution (12-bits) and 13 spectral bands, including four visible and SWIR  
98 channels (Drusch et al., 2012). Inland water *TSI* has been produced for large lakes using  
99 MODIS sensor (Wang et al 2018). However, this study is for more than 2000 large lakes  
100 (due to the spatial resolution of the sensor) while there are 117 million of lakes on Earth  
101 (Verpoorter et al. 2014). The Copernicus Land Monitoring Service has started to  
102 produce *TSI* for lakes large enough to be mapped with 100 m pixel size using Sentinel-2



103 MSI. However, this product is available only for Europe and some parts of Africa.

104           Instead of individual parameters, several studies (e.g., Morel and Prieur, 1977;  
105 Gurlin et al., 2011; Huang et al., 2014; Sass et al., 2007; Thiemann & Kaufmann, 2000;  
106 Yin et al. 2018) have also provided empirical relationships expressed as band  
107 combinations or baseline methods to acquire Chl-a, Secchi or nutrients related to  
108 potential *TSI* calculations in regional lakes. However, the accuracy of these empirical  
109 relationships for transferring knowledge from some representative lakes to large-scale  
110 lake groups is limited by large uncertainties (i.e., in areas with different water quality  
111 concentrations and atmospheric component influences, fewer lakes can be used with  
112 more heterogeneous influences and uniform algorithms) (Oliver et al., 2017).  
113 Considering the requirement of a uniform and universal relationship to quantify the  
114 trophic status of lakes, an alternative method using high-frequency and spatial  
115 resolution of the sensor is a significant challenge. Recently, technological developments,  
116 such as machine learning algorithms, have allowed the usage of remotely sensed  
117 imagery to successfully investigate water quality parameters using artificial intelligence  
118 (Reichstein et al., 2019; Pahlevan et al., 2020; Cao et al., 2020). The potential  
119 application and development of machine learning for remote quantification of water  
120 quality is attributed to the following advantages: requirement of little prior knowledge,  
121 rich features can be captured, and robust relationships can be obtained. These processes  
122 avoid bias and uncertainty from the regional environmental background as well as  
123 complications due to atmospheric components of traditional remote sensing-derived  
124 relationships over large-scale, i.e. for multiple lakes. Given the novel application of  
125 remote sensing and machine learning, this is a gap to fill for large-scale research of  
126 monitoring trophic states.

127           Environmental issues fueled by rapid economic growth in China have significantly



128 increased in the last three decades. Lake eutrophication is a serious issue, with large  
129 variability in terms of trophic status and optical properties. However, most studies (Jin,  
130 2003, 2005; Fragoso et al., 2011; Huang et al., 2014) have addressed eutrophication  
131 concerns in only a single lake or two lakes since the 1990s. It is acknowledged that a  
132 rapidly growing economy and anthropogenic activities (e.g., elevated nutrient loading  
133 and increasing air pollution) accelerate the aging process of lakes (Wu et al., 2011; Shi  
134 et al., 2020). Therefore, it is critical to objectively assess the trophic status and pay  
135 attention to protect the aquatic environment. We aim to provide a robust machine  
136 learning algorithm and remote sensing flowchart from simultaneously retrieved *TSI*  
137 over a wide range of bio-optical compositions in different lakes. The objectives of our  
138 study were to: (1) examine biogeochemical parameters and assess trophic status, (2)  
139 calibrate and validate the *TSI* model using different machining learning algorithms from  
140 MSI-imagery derived remote sensing reflectance spectra (*Rrs*), with different lake  
141 classifications; and (3) quantify and map the trophic status of typical 555 lakes in five  
142 Chinese limnetic regions.

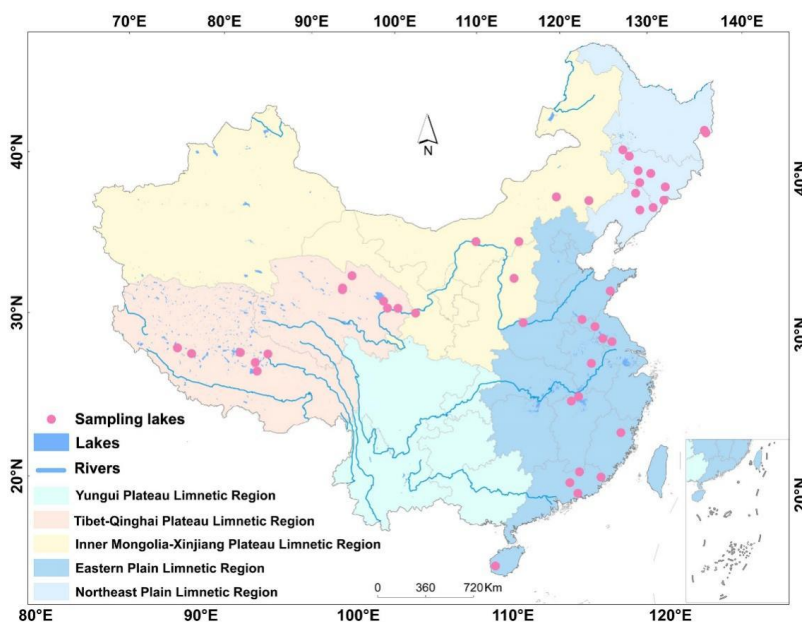
## 143 **2 Materials and methods**

### 144 **2.1 Study area and sampling process**

145 China is located in the east of Asia with a land area of 9,600,000 square kilometers  
146 and a population of over 1.4 billion. The terrain of China descends from west to east in  
147 three steps. Due to a vast territory span, this country has diverse climatic, geographical,  
148 and geological conditions. There are 2,693 natural lakes (with area >1.0 km<sup>2</sup>) that are  
149 distributed in China (Ma et al., 2011). Protection and sustainable management of these  
150 lakes have been priorities, considering the degradation of water quality over several  
151 decades. In this study, a total of 45 lakes were visited and 431 samples were collected in  
152 early April 2016 to late October 2019 (Table S1 and Fig. 1), which was the highest



153 productive season, as identified by Carlson's *TSI* model. These datasets were analyzed  
154 and published in (Li et al., 2021; Song & Li et al., 2019; Song et al., 2020). Our lake  
155 dataset was collected from various types of lakes across China, and efforts were made to  
156 examine lake trophic status from a wide range of water quality parameters, lake sizes  
157 (0.5 to 4, 256 km<sup>2</sup>), lake elevation (10 to 4, 525 m), and climatic zones (Song and Li et  
158 al., 2019). In the field, some lakes were sampled in the middle while others were  
159 sampled at multiple locations evenly distributed over the lake. The water samples were  
160 collected approximately 0.5 m below the surface, and then stored in 1 L amber HDPE  
161 bottles and kept in a portable refrigerator (4°C) before being transported to the  
162 laboratory. During the sampling process, the Secchi disk depth (SDD, m) was measured  
163 using a black-and-white Secchi disk. The pH and electrical conductivity (EC,  $\mu\text{s cm}^{-1}$ )  
164 were recorded using a portable multi-parameter water quality analyzer (YSI 6600, 170  
165 U.S).



166

167

**Figure 1: Location of lake sites.**



168 **2.2 Laboratory analysis**

169 A transferred portion of each bulk water sample was immediately filtered with  
170 0.45- $\mu\text{m}$  pore size Whatman cellulose acetate membrane filters in the laboratory. It is to  
171 be noted that some remote Tibet and Qinghai lake samples had to be filtered during  
172 fieldwork. Chlorophyll-a (Chl-a) was extracted from the filters using a 90 % buffered  
173 acetone solution at 4 ° C under 24 h dark conditions. According to the SCOR-UNESCO  
174 equations (Jeffrey and Humphrey, 1975), the concentration of Chl-a ( $\mu\text{g L}^{-1}$ ) was  
175 determined using a UV-2600PC spectrophotometer at 750 nm, 663 nm, 645 nm, and  
176 630 nm. Dissolved organic carbon ( $\text{mg L}^{-1}$ ) concentrations were determined using a  
177 total organic carbon analyzer. Total nitrogen (TN) and total phosphorus (TP)  
178 concentrations ( $\text{mg L}^{-1}$ ) were measured using a continuous flow analyzer (SKALAR,  
179 San Plus System, the Netherlands) using a standard procedure (APHA/AWWA/WEF,  
180 1998). In addition, total suspended matter (TSM,  $\text{mg L}^{-1}$ ) concentrations were obtained  
181 gravimetrically using pre-combusted 0.7- $\mu\text{m}$  pore size Whatman GF/F filters. All  
182 preprocesses (e.g., filtration and concentration quantification) of all water samples were  
183 undertaken within two days in the laboratory. The procedures are provided in detail in  
184 Li et al. (2021).

185 The bulk samples were again filtered through a 0.7- $\mu\text{m}$  pore size glass fiber  
186 membrane (Whatman, GF/F 1825-047) to retain particulate matter. The water from  
187 particulate matter measurements was then filtered through a 0.22- $\mu\text{m}$  pore size  
188 polycarbonate membrane (Whatman, 110606) in order to measure chromophoric  
189 dissolved organic matter (CDOM) absorption of each sample. According to the  
190 quantitative membrane filter technique (Cleveland and Weidemann, 1993), the light  
191 absorption of total particulate matter  $a_p(\lambda)$  can be separated into phytoplankton pigment  
192 absorption  $a_{ph}(\lambda)$ , non-algal particles  $a_d(\lambda)$ , and CDOM absorption  $a_{CDOM}(\lambda)$ . The optical





193 density (OD) of the particulate matter retained in the filters was measured using a  
194 UV-2600PC spectrophotometer at 380–800 nm, with a blank membrane as a reference  
195 at 380–800 nm. The filters were then bleached using a sodium hypochlorite solution to  
196 remove phytoplankton pigment and measured again using a spectrophotometer. Finally,  
197 the phytoplankton pigment absorption  $a_{ph}(\lambda)$  was calculated by subtracting  $a_d(\lambda)$  from  
198 the total particulate matter  $a_p(\lambda)$ . The absorption coefficients of the optical active  
199 substance (OACs) were calculated according to Song et al. (2013).

### 200 **2.3 Trophic status assessment of lakes**

201 Several studies have proposed different indices of the lake trophic state (Aizaki et al.,  
202 1981; Carlson, 1977). Carlson's trophic state index used five variables, such as Chl-a,  
203 TP, TN, SDD, and chemical oxygen demand (COD), to characterize the trophic state.  
204 However, there are no optical characteristics for TN, TP and COD to manifest in  
205 changes of remote sensing reflectance, which may bring more uncertainties or errors.  
206 Thus, Chl-a, TP, and SDD were selected to assess the trophic status according to the  
207 modified Carlson's trophic state index (*TSI*). The *TSI* can be calculated using individual  
208  $TSI_M(\text{Chl-a})$ ,  $TSI_M(\text{SDD})$ , and  $TSI_M(\text{TP})$  using the following equations:

$$209 \quad TSI_M(\text{Chl-a}) = 10 \times \left( 2.46 + \frac{\ln \text{Chl-a}}{\ln 2.5} \right) \quad (1)$$

$$210 \quad TSI_M(\text{SDD}) = 10 \times \left( 2.46 + \frac{3.69 - 1.52 \times \ln \text{SDD}}{\ln 2.5} \right) \quad (2)$$

$$211 \quad TSI_M(\text{TP}) = 10 \times \left( 2.46 + \frac{6.71 + 1.15 \times \ln(\text{TP})}{\ln 2.5} \right) \quad (3)$$

$$212 \quad TSI = 0.54 \times TSI_M(\text{Chl-a}) + 0.297 \times TSI_M(\text{SDD}) + 0.163 \times TSI_M(\text{TP}) \quad (4)$$

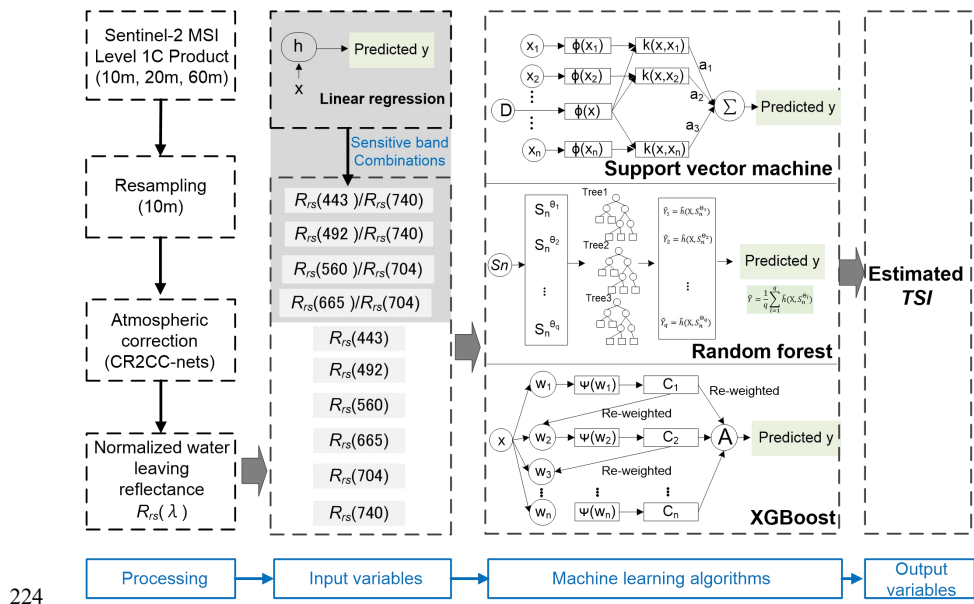
213 Where, the *TSI* below 30 correspond to oligotrophic waters, above 50 are eutrophic and  
214 *TSI* between 30 and 50 in mesotrophic (Carlson, 1977).

### 215 **2.4 Multi-Spectral Instrument imagery and atmospheric correction**

216 Sentinel-2A/B MSI imagery was acquired from the Copernicus Open Access Hub



217 of the European Space Agency. Altogether, 210 scenes of cloud-free Level-1C images  
 218 covering the lakes were downloaded with a time window of  $\pm 7$  days from in situ  
 219 measurements. The Case 2 Regional Coast Color processor (C2RCC) was used to  
 220 remove atmospheric effects. An average of 3×3-pixels centered at each in situ sampling  
 221 station was used in the further analysis. All the processes were performed using the  
 222 Sentinel Application Platform (SNAP) version 7.0.0. A flowchart of the process is  
 223 shown in Fig. 2.



225 **Figure 2 : Workflow of the Sentinel-2 MSI data and machine learning algorithms**  
 226 **for estimating TSI**

227  
 228 **2.5 Machine learning algorithms**

229 As a branch of artificial intelligence, the application of machine learning is  
 230 growing in the field. Machine learning can automatically analyze huge chunks of data,  
 231 develop optimal models, generalize algorithms, and make predictions. These approaches  
 232 have been applied in a variety of eco-environmental and remote sensing fields  
 233 (Mountrakis et al., 2011; Pahlevan et al., 2019). Hence, we employed four



234 representative machine learning algorithms, namely linear regression (LR), support  
235 vector machine (SVM), XGBoost (XGB), and random forest (RF) (Supplementary data,  
236 methods), to establish a *TSI* model. To strengthen the robustness, band combinations  
237 sensitive to *TSI* were determined by LR (Fig. 2), and were added to the procedure of  
238 machine learning algorithms as input variables. Subsequently, the output variable was  
239 the predicted *TSI*. The in situ measured samples were then randomly divided into a  
240 calibration dataset (70%, 287 lake samples) and validation dataset (30%, 144 lake  
241 samples) using MATLAB software. The *TSI* modeling procedure considering machine  
242 learning and Multiple Linear Regression (MLR) was processed using the R software.

## 243 **2.6 Classifications of lakes**

244 In order to provide further feasibility for the application and availability of the *TSI*  
245 model, the in situ measured samples were classified in three ways (Fig. 3):

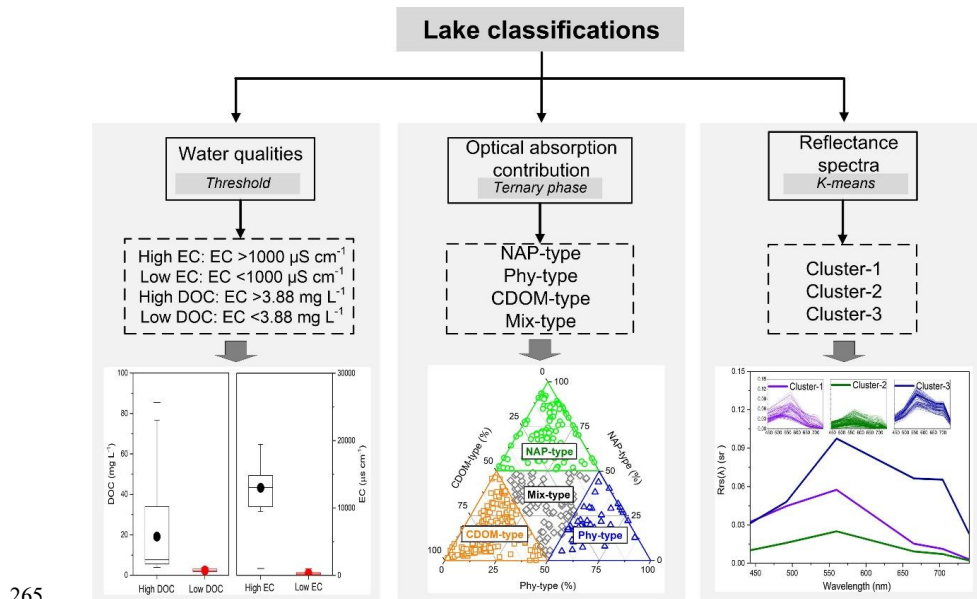
246 a) based on water quality: Salinity classification referred to the threshold value of  
247 electrical conductivity (named EC,  $EC=1000 \mu\text{S cm}^{-1}$ ) (Duarte et al., 2008), following  
248 which the lakes were divided into brackish lakes ( $N=100$  samples) and fresh water lakes  
249 ( $N=331$  samples). Dissolved organic carbon (DOC) in global lake water classification  
250 referred to the volume weighted averaged DOC level of global lakes ( $3.88 \text{ mg L}^{-1}$ )  
251 according to Toming et al., (2020), following which lakes were divided into high DOC  
252 lake ( $N=224$  samples) and low DOC lake ( $N=207$  samples).

253 b) based on optical absorption contribution: Optical absorption classification  
254 referred to Prieur and Sathyendranath (1981), where the total light absorption of water  
255 can be separated from phytoplankton pigment absorption, non-algal particles, and  
256 CDOM absorption, respectively. The relative percentage of absorption contribution of  
257 OACs can be divided into phytoplankton-type (Phy-type) lakes ( $N=54$  samples),  
258 non-algal particles-type (NAP-type) lakes ( $N=109$  samples), CDOM-type lakes ( $N=177$



259 samples), and mix-type lakes ( $N=91$  samples).

260 c) based on reflectance spectra: In order to discern the different optical  
261 characteristics of lakes, the derived MSI reflectance was clustered using the k-means  
262 clustering approach with a gap statistic (Neil et al., 2018). We identified 431 MSI  
263 reflectance  $Rrs(\lambda)$  spectra for three branches (Table S3), and the  $Rrs(\lambda)$  spectra are  
264 shown in Fig.3.



265  
266 **Figure 3: Lake classifications considering three ways, i.e., water quality, optical**  
267 **absorption contribution and reflectance spectra. ANOVA analysis was conducted**  
268 **in different classifications ( $p<0.001$ ) (Table S3).**

### 269 2.7 Statistical analyses and accuracy assessment

271 Statistical analysis, including descriptive statistics, correlation ( $r$ ), regression ( $R^2$ ),  
272 and ANOVA analyses, were implemented with Statistical Program for Social Science  
273 software (version 16.0; SPSS, Chicago, IL, USA). Correlation and regression analyses  
274 were used to examine the relationships between the water quality parameters and  
275 absorption coefficients of OACs as well as the  $TSI$  model calibration and validation.  
276 The differences in trophic status, EC classification, DOC classification, absorption



277 coefficients of OAC classification, and MSI reflectance spectra classification for *TSI*  
278 model validation were assessed using one-way ANOVA. The significance level was set  
279 at  $p < 0.05^*$ . The mean normalized error (MAE) and root mean square error (RMSE)  
280 were used to assess the performance of the *TSI* model (Supplementary data, accuracy  
281 assessment).

## 282 **3 Results**

### 283 **3.1 Aquatic environmental scenery**

284 The water quality and bio-optical properties covered a wide range of nutrient  
285 compositions, transparencies, and trophic states, revealing different geographical  
286 environmental scenery (Tables S1 and S2-4). The EC and DOC concentration showed  
287 high variability, ranging for example, from 3345.31  $\mu\text{s cm}^{-1}$  (TuoSu, TS20) in  
288 Tibet-Qinghai region to 0.17  $\mu\text{s cm}^{-1}$  (Qingnian, QN2) in Northeast region. For the  
289 water quality parameters to characterize *TSI*, the Chl-a concentration ranged from 0.12  
290 to 100.22  $\mu\text{g L}^{-1}$ , with the highest value recorded in TaiPingChi (TPC5) and the lowest  
291 value in Namoco (NMC36). The range of TP was from 0.003  $\text{mg L}^{-1}$  (Erlong, EL8) to  
292 2.17  $\text{mg L}^{-1}$  (Dali, DL7), and SDD ranged from 0.17 m (Chalhu, CH32) to 9.47 m  
293 (NMC36) for surveyed lakes, respectively. Overall, the maximum values of EC, DOC,  
294 turbidity, Chl-a, TSM, and SDD were 196782.35, 948.4, 723.3, 770.92, 614.58, and  
295 55.71 fold greater than the minimum values, respectively, indicating that our dataset  
296 was representative of diverse water qualities.

297 Lake samples were grouped into different classifications based on water quality  
298 (e.g., EC and DOC), optical absorption contribution, and reflectance spectra (Table 1  
299 and Fig. 3). The results indicated that all water qualities showed significant differences  
300 ( $p < 0.05$ ) under different lake classifications. For example, brackish lakes showed higher  
301 average values of SDD, TP, DOC, and optical attributions of OAC values than those of



302 fresh water lakes, but the turbidity, Chl-a, and TSM concentrations were lower. Lakes  
303 equipped with low DOC levels had a low average value of SDD than that of lakes with  
304 high DOC levels. NAP-type lakes exhibited the highest average Chl-a and DOC values,  
305 whereas Phy-type lakes had the highest average turbidity and TSM values, and the  
306 highest average SDD and TP values were recorded in CDOM-type and Mix-type lakes,  
307 respectively. For reflectance spectra classifications (Fig. 3), the highest average EC,  
308 SDD, and DOC were recorded in cluster-1 lakes, the highest average turbidity and TP  
309 was shown in cluster-3 lakes and the highest average TSM was found in cluster-2 lakes.



310

**Table1 (a) Averaged values (Avg.) of water quality and bio-optical properties considering lake classifications and (b) ANOVA analysis (*F* value) among them**

Lake classifications	<i>N</i>	EC	Turbidity	SDD	Chl-a	TP	DOC	TSM	$\alpha_{ph}(440)$	$\alpha_d(440)$	$\alpha_{CDOM}(440)$
(a)	Brackish	100	12986.28	8.83	2.21	4.18	33.31	8.42	0.23	0.27	0.42
	Fresh	331	302.39	21.75	1.43	8.58	4.28	19.52	0.56	1.13	0.57
	High DOC	224	5988.93	23.90	1.39	10.42	19.07	21.50	0.68	1.14	0.65
	Low DOC	207	276.19	12.45	1.85	4.46	2.29	11.98	0.27	0.71	0.41
	NAP-type	54	5156.02	11.28	1.58	14.26	18.75	15.99	1.29	0.41	0.55
	Phy-type	109	825.48	43.28	0.65	6.85	4.75	37.18	0.46	2.74	0.49
	CDOM-type	177	4081.96	4.44	2.43	3.64	9.70	4.99	0.13	0.15	0.51
	Mix-type	91	3424.07	19.40	1.17	12.05	16.48	16.22	0.70	0.60	0.62
	Cluster-1	87	6948.28	4.46	2.38	2.64	17.92	5.76	0.26	0.17	0.28
	Cluster-2	215	2728.71	6.18	2.05	8.57	7.18	5.81	0.35	0.36	0.52
Cluster-3	129	1626.05	46.68	0.36	9.19	12.73	42.59	0.84	2.39	0.73	
(b)	Brackish	100	-	18.7**	21.8**	12.0**	68.9**	20.4**	16.6**	29.8**	9.6*
	Fresh	331	-	19.8**	10.0**	32.2**	23.3**	21.0**	38.0**	10.0*	39.3**
	High DOC	224	93.8**	71.6**	46.0**	21.0**	13.5**	73.0**	-	-	-
	Low DOC	207	7.4**	17.9**	25.2**	11.0**	18.5**	18.9**	26.1**	171.4**	33.5**
	NAP-type	54	-	17.9**	25.2**	11.0**	18.5**	18.9**	26.1**	171.4**	33.5**
	Phy-type	109	7.4**	71.6**	46.0**	21.0**	13.5**	73.0**	-	-	-
	CDOM-type	177	-	17.9**	25.2**	11.0**	18.5**	18.9**	26.1**	171.4**	33.5**
	Mix-type	91	-	17.9**	25.2**	11.0**	18.5**	18.9**	26.1**	171.4**	33.5**
	Cluster-1	87	-	17.9**	25.2**	11.0**	18.5**	18.9**	26.1**	171.4**	33.5**
	Cluster-2	215	220.9**	17.9**	25.2**	11.0**	18.5**	18.9**	26.1**	171.4**	33.5**
Cluster-3	129	-	17.9**	25.2**	11.0**	18.5**	18.9**	26.1**	171.4**	33.5**	

The unit of TN, TP, DOC and TSM is  $\mu\text{g L}^{-1}$ ; EC is  $\mu\text{s cm}^{-1}$ ; Chl-a is  $\mu\text{g L}^{-1}$ ; turbidity is NTU (nephelometric turbidity unit). Significance levels are reported as significant (noted with \*, 0.05 >  $p$  > 0.01) or highly significant (noted with \*\*,  $p$  < 0.01).

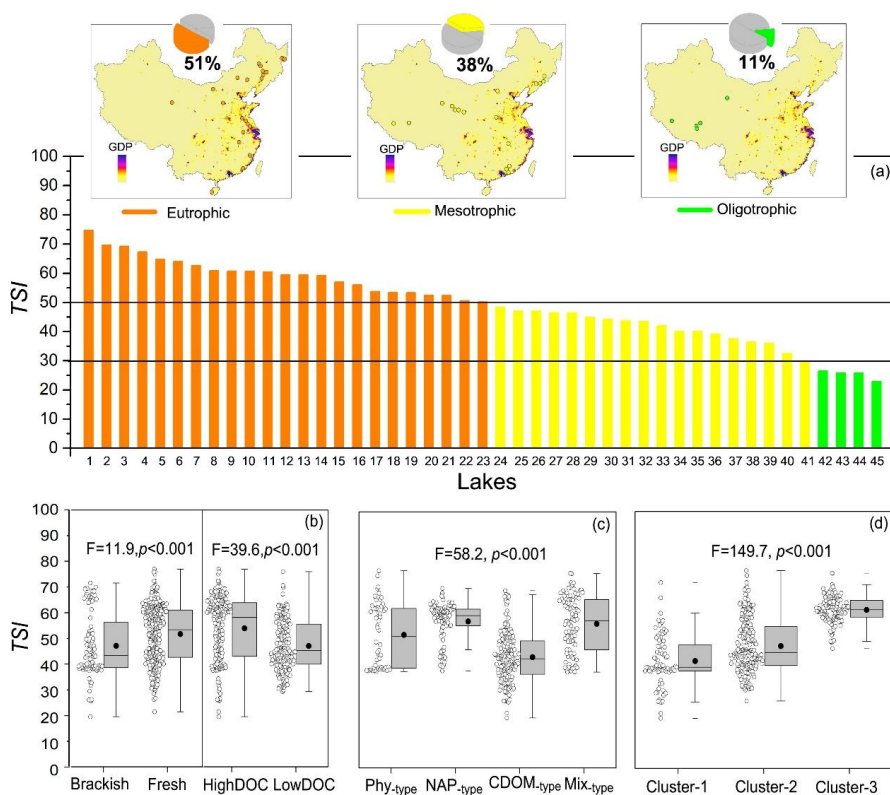


311

### 312 **3.2 Trophic status assessment**

313 The trophic status of 45 lakes across China, from where in situ samples were  
314 collected, was evaluated (Fig. 4a). Our results showed that there were 13 oligotrophic  
315 (3.02 %), 199 mesotrophic (46.17 %), and 219 eutrophic (50.81 %) samples. Because  
316 our samples were collected in different seasons and eutrophication is time-dependent,  
317 the *TSI* values of samples within a lake were averaged. It can be shown that only five  
318 lakes accounting for 11.1% of investigated lakes were characterized with an  
319 oligotrophic status, 17 lakes accounting for 37.8 % were mesotrophic, and 23 lakes  
320 accounting for 51.1 % were characterized with eutrophic status. These eutrophic lakes  
321 were distributed in the eastern region of China (Fig. 4b), and were associated with a  
322 highly concentrated human population and economic development. Moreover, the  
323 ANOVA results showed that the *TSI* of lake samples were significantly different  
324 considering lake classifications (Fig. 4c, and d).





325

326 **Figure 4:** (a) is the averaged *TSI* in collected samples from lakes across China and  
 327 their spatial distribution. The number of lakes can be found in TableS1. The box  
 328 plots of *TSI* at different classifications of water quality (b), optical absorption  
 329 contribution types (c) and reflectance spectra (d). The balls beside the boxes are  
 330 the lake samples, and the black balls in the boxes represent the mean values. The  
 331 horizontal edges of the boxes denote the 25th and 75th percentiles; the whiskers  
 332 denote the 10th and 90th percentiles.

333

334

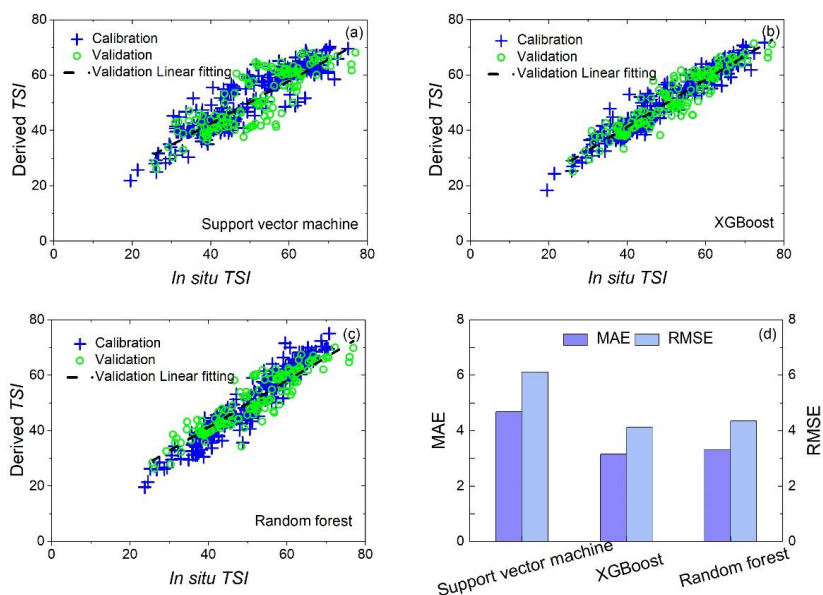
### 3.3 Calibration and validation of *TSI* model

335

In this section, multiple linear regression was used to identify significantly  
 336 sensitive spectral variables related to *TSI* (Table 2 and Fig. 2). Of the band combinations  
 337 validated in the study ( $N=144$ ), the blue/red [ $Rrs(443)/Rrs(740)$ ,  $Rrs(492)/Rrs(740)$ ],  
 338 and green/red [ $Rrs(560)/Rrs(704)$ ,  $Rrs(665)/Rrs(704)$ ] band ratios showed a good  
 339 regression coefficient ( $R^2>0.59$ ) with *TSI*. These band combinations provided certain  
 340 sensitive spectral variables that responded to the lake eutrophic status. Hence, to



341 strengthen the robustness of the three machine learning models, the blue/red and  
342 green/red combinations above were considered as the input variables as well as six  
343 spectral variables ( $Rrs(\lambda)$  at 443, 492, 560, 665, 709, and 740 nm). Likewise, the output  
344 variables were estimated using  $TSI$  to examine the performances (Fig. 5). The results  
345 showed that when XGBoost was applied to the validation data ( $N=144$ ), the  
346 performance of the model was excellent ( $R^2=0.87$ , slope=0.85) with low errors (MAE=  
347 3.15, RMSE=4.11). The support vector machine ( $R^2=0.71$ , slope=0.77, MAE=4.67,  
348 RMSE=6.11) and random forest ( $R^2=0.85$ , slope=0.84, MAE=3.31, RMSE=4.34)  
349 models also showed significant performance. These results demonstrate the potential of  
350 using XGBoost by considering band combinations to derive  $TSI$  from Sentinel products.



351

352 **Figure 5: Relationships between in situ and derived TSI for both model training**  
353 **and testing samples by support vector machine (a), XGBoost (b) and random**  
354 **forest (c), as well as their errors (d).**

355

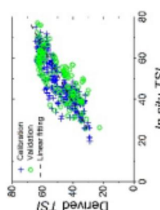
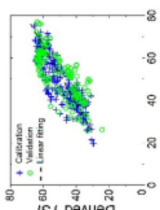
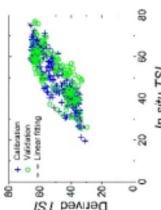
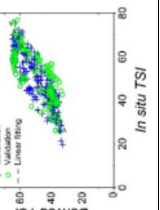
356

357

358

359  
 360

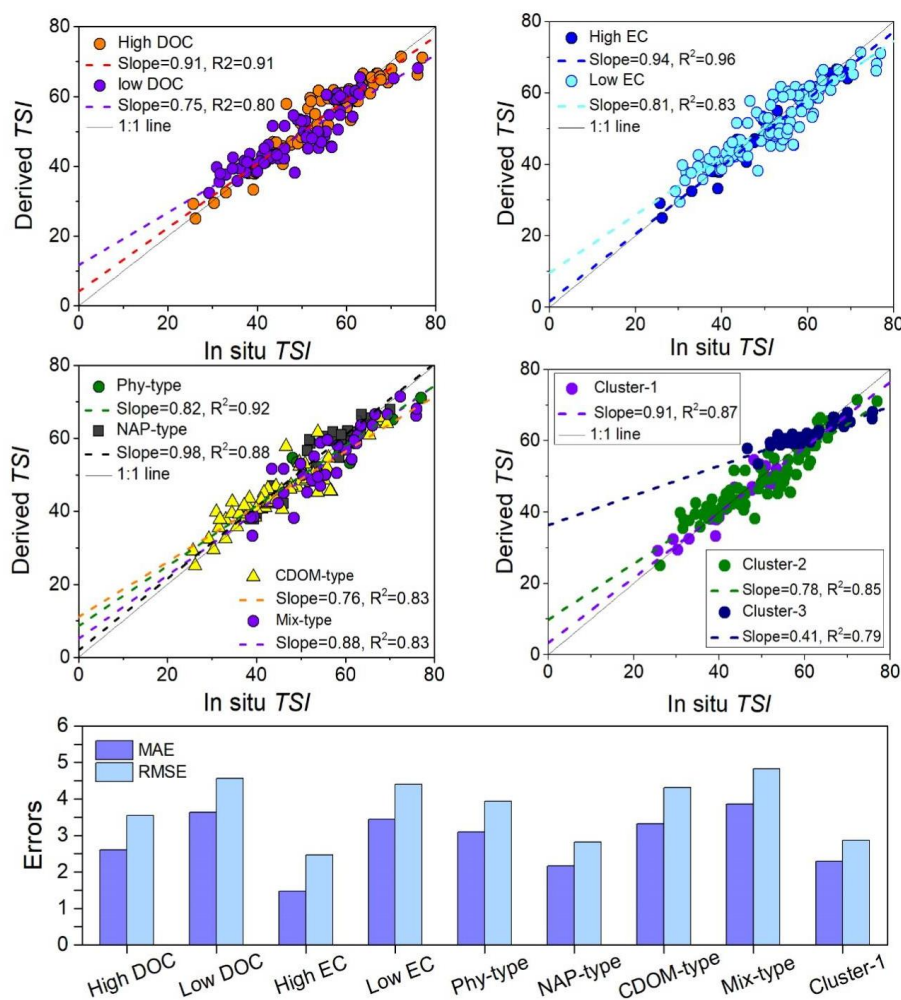
**Table 2** Multiple linear regression between measured- and estimated-  $TSI$  from the MSI spectral bands after using CR2CC processor

Band combinations	Datasets	$N$	Fitting equation	$R^2$	Errors	Plots figures
Band 1/ Band 6 (Blue/Red)	Calibration	287	$TSI = -8.5 \ln [Rrs(B1)/Rrs(B6)] + 63.47$	0.7	MAE = 6.45	
	Validation	144	$TSI_{derived} = 0.73 \times TSI_{in situ} + 11.868$	6	RMSE = 5.85	
				0.6	MAE = 6.26	
				1	RMSE = 7.48	
Band 2/ Band 6 (Blue/Red)	Calibration	287	$TSI = -8.87 \ln [Rrs(B2)/Rrs(B6)] + 67.91$	0.7	MAE = 4.57	
	Validation	144	$TSI_{derived} = 0.74 \times TSI_{in situ} + 11.751$	7	RMSE = 5.74	
				0.6	MAE = 6.32	
				0	RMSE = 7.57	
Band 3/ Band 5 (Green/Red)	Calibration	287	$TSI = -13.63 \ln [Rrs(B3)/Rrs(B5)] + 67.26$	0.7	MAE = 4.55	
	Validation	144	$TSI_{derived} = 0.72 \times TSI_{in situ} + 12.44$	7	RMSE = 5.70	
				0.5	MAE = 6.39	
				9	RMSE = 7.66	
Band 4, Band 5 (Red/Red)	Calibration	287	$TSI = -44.15 \times [Rrs(B4)/Rrs(B5)] + 108$	0.8	MAE = 4.39	
	Validation	144	$TSI_{derived} = 0.72 \times TSI_{in situ} + 12.32$	0	RMSE = 5.43	
				0.5	MAE = 6.85	
				9	RMSE = 7.94	



361 **3.4 *TSI* model application to lake classifications**

362 The *TSI* model calculated by XGBoost was assessed by comparing derived and in  
363 situ *TSI* considering different lake classifications (Fig. 6). We aimed to provide a  
364 universal *TSI* model and evaluate its feasibility in different aquatic environments.  
365 Significant agreement (slope>0.91,  $R^2>0.91$ ) between derived and in situ *TSI* was  
366 observed in lakes with high DOC levels (DOC>3.88 mg L<sup>-1</sup>) and EC values (EC>1000  
367  $\mu\text{S cm}^{-1}$ ), with low errors. For lakes classified by different absorption contributions, the  
368 NAP-type (slope=0.98,  $R^2=0.88$ ) and Phy-type (slope=0.82,  $R^2=0.92$ ) samples generally  
369 showed a positive derived performance than those of Phy-type, CDOM-type, and  
370 Mix-type, respectively. In addition, a significant relationship between derived and in  
371 situ *TSI* can be described for lakes with cluster-1 reflectance spectra, with slope=0.91,  
372  $R^2=0.87$ , RMSE=2.87, and MAE=2.29.



373

374 **Figure 6:** Scatter plots of derived- and in situ-TSI by XGBoost for validation  
 375 samples ( $N=144$ ) according to lake classifications, such as water quality (DOC and  
 376 EC) (a-b), absorption contribution (c), reflectance spectra(d) with the 1:1 line (red  
 377 solid) and errors (e).

378

### 379 3.5 Spatio-temporal patterns of trophic states in a large-scale overview

380 Previous studies have demonstrated that some lakes disappeared or increased

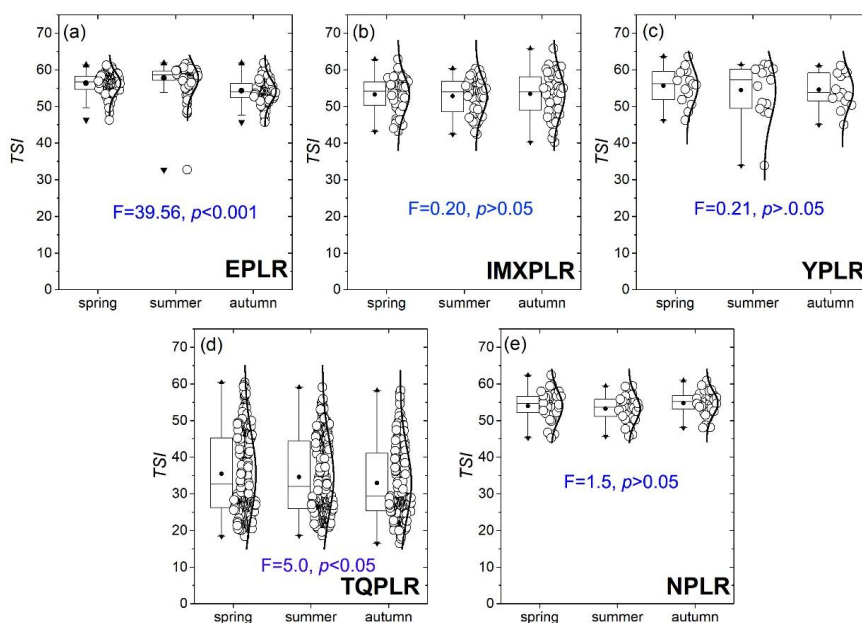
381 numbers recently according to statistics from Ma et al. (2011). Thus, we selected some

382 representative lakes ( $N=555$ ) to qualify spatiotemporal trophic states using the XGBoost

383 algorithm. According to the different geographic and limnological types in China, lakes



384 were divided into five limnetic regions (Wang and Dou 1998, Early National  
385 Investigation): Eastern Plain Limnetic Region (EPLR,  $N=123$ ), Northeast Plain  
386 Limnetic Region (NPLR,  $N=37$ ), Inner Mongolia-Xinjiang Plateau Limnetic Region  
387 (IMXPLR,  $N=56$ ), Yungui Plateau Limnetic Region (YGPLR,  $N=15$ ), and  
388 Tibet-Qinghai Plateau Limnetic Region (TQPLR,  $N=324$ ) (Fig. 1 and Supplementary  
389 data). In general, there were significant seasonal variations in eutrophic state for lakes  
390 from the EPLR ( $F=39.56$ ,  $p<0.001$ ) and TQPLR ( $F=5.0$ ,  $p<0.05$ ) (Fig. 7). The eutrophic  
391 lakes dominated the proportions of the investigated lakes in the EPLR (93.5 %),  
392 followed by the NPLR (89.2 %) and YGPLR (86.7 %). In comparison, most  
393 mesotrophic and oligotrophic lakes were distributed in the TQPLR. The spatio-temporal  
394 patterns of trophic states in lakes were related to lake basin characteristics, climate, and  
395 anthropogenic activities.

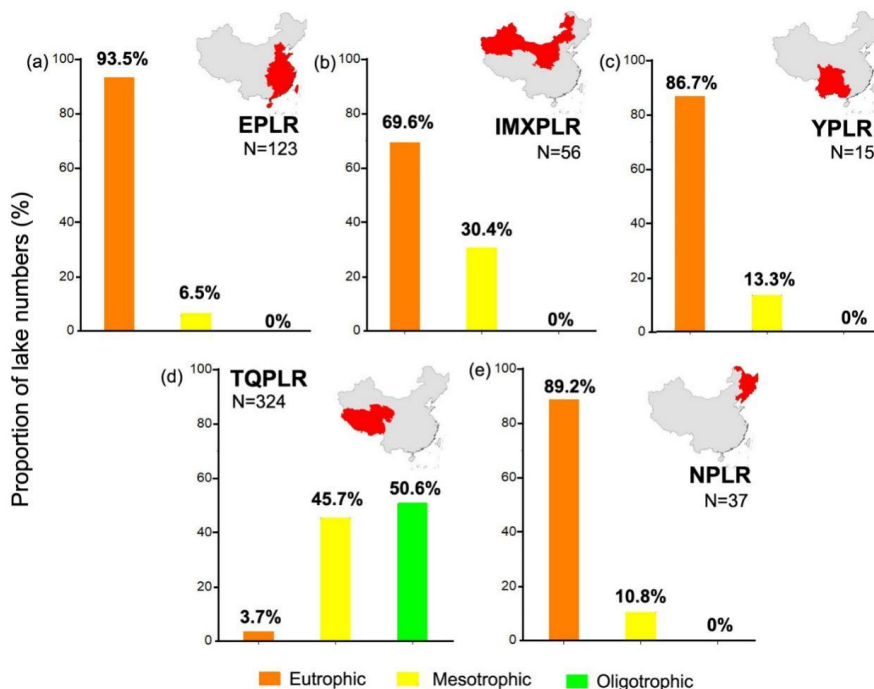


396

397 **Figure 7 : Box plots of TSI derived from XGBoost model in investigated lakes**  
398 **from the five limnetic regions (Wang & Dou 1998), i.e., (a) EPLR, (b) IMXPLR, (c)**  
399 **YPLR, (d) TQPLR and (e) NPLR. The black line and balls in the boxes represent**



400 the median and mean values, respectively. The horizontal edges of the boxes denote  
401 the 25th and 75th percentiles; the whiskers denote the 10th and 90th percentiles.  
402



403

404 **Figure 8** : The proportions of lake numbers (%) for different trophic state in the  
405 five limnetic regions (Wang & Dou 1998), i.e., (a) EPLR, (b) IMXPLR, (c) YPLR,  
406 (d) TQPLR and (e) NPLR. N represents the lake numbers.  
407

## 408 4 Discussion

### 409 4.1 Remote-sensed and machine-learning-based *TSI* model

410 Traditional approaches to quantitatively characterize the trophic status rely on field  
411 measurements of trophic parameters, for example, Chl-a, nutrients, and SDD, to  
412 calculate the *TSI* (Carlson, 1977). It is difficult and costly to make field measurements  
413 in lakes in remote locations. The *TSI* calculation does not need all of these trophic  
414 parameters but just one, for example, Chl-a (Thiemann and Kaufmann, 2000), SDD  
415 (Olmanson et al., 2008; Song et al., 2020), TP (Kutser et al., 1995) and total absorption  
416 coefficients (Lee et al., 1999; Shi et al., 2019), etc. There have been many lake studies



417 (Chl-a and SDD, Sheela et al., 2011; Chl-a, SDD and TP, Song et al., 2012) where two  
418 or three water quality parameters were mapped, which would allow to subsequently  
419 gather them to calculate comprehensive *TSI*. Although these studies provided the  
420 potential to evaluate the trophic status of lakes, *TSI* is a synthetic indicator that is  
421 affected by biological, physical, and chemical factors that co-vary in most instances.  
422 Huang et al. (2014) also tried to derive *TSI* using remote sensing spectrum reflectance,  
423 but the accuracy was not completely usable. It shows that variability in remote sensing  
424 estimates of the *TSI* are not bad.

425 With advances in artificial intelligence technology and the increasing use of  
426 computer applications in recent years, machine learning has become a useful tool for  
427 monitoring aquatic environments by remote sensing (Mountrakis et al., 2011). It allows  
428 us to develop and evaluate a machine-learning-based *TSI* model that addresses quality  
429 and accuracy problems more effectively (Li et al., 2021). Hence, we propose a new  
430 approach to directly characterize the trophic status and accurately reflect spatial  
431 variations in this study, but should also be conveniently available for the different lake  
432 classifications (Figs. 5, 6). Using machine learning algorithms, in order to improve the  
433 robustness and applicability of the *TSI* model, a sufficient database of trophic state  
434 parameters ( $N=431$ ) was collected from lakes with different biogeochemical  
435 characteristics, such as water quality, absorption contributions of different optically  
436 active substances, and reflectance spectra (Table1). We first used B1-B6 reflectance as  
437 input variables of machine learning algorithms, and XGBoost showed a significant  
438 performance with  $R^2$  and a slope of 0.85 (Fig. S1). The support vector machine and  
439 random forest did not produce the sufficient performance. There was no optical  
440 response bands or appropriate band ratios for *TSI*. We thus used a multiple linear  
441 regression to find some suitable sensitive band combinations responding to the *TSI*,





442 which made it possible to develop a robust machine-learning-based *TSI* model. It is  
443 important to note that the blue/red [ $Rrs(443)/Rrs(740)$ ,  $Rrs(492)/Rrs(740)$ ], and  
444 green/red [ $Rrs(560)/Rrs(704)$ ,  $Rrs(665)/Rrs(704)$ ] band ratios were significantly  
445 correlated with *TSI* (Table 2). This result indicated that the blue/red and green/red band  
446 ratios were more sensitive to the *TSI*, although the nutrients and SDD had no optical  
447 response. It was known for decades that the blue part of spectrum is useless when water  
448 itself is not blue (i.e. outside of ocean or very oligotrophic mountain lakes), owing to  
449 the noneffective atmospheric correction and complex reflectance signals. However, our  
450 dataset to train *TSI* models contain the samples from blue and oligotrophic Tibetan lakes,  
451 which are like the oceanic environments (Liu et al., 2021). The blue bands responding  
452 to *TSI* were thus used in this study. Most empirical Chl-a estimation studies adopted  
453 red/near infrared (NIR) band ratios to calibrate models using reflectance signatures  
454 (Gitelson et al., 1992). Similarly, empirical SDD retrieval models provided by previous  
455 studies used empirical algorithms or models to figure out what bands should work the  
456 best considered the following ratios: blue/green, red/blue plus red/green, and red/blue  
457 plus blue (Bindling et al., 2007), and Red/Blue ratio plus Blue (Kloiber et al., 2002).  
458 Kutser et al. (1995) also built a TP retrieval model using the red and NIR ratios, which  
459 is consistent with Chl-a empirical models. Overall, it is not surprising for our *TSI* model  
460 to have strong correlations with the blue/red and green/red band ratios because the *TSI*  
461 incorporates the optical properties.

462 For this reason, we used MSI bands in the visible band ratios at six bands,  
463 considering the comprehensive spectrum information about the trophic status of lakes as  
464 input variables (Fig. 2). The three representative machine learning *TSI* models improved  
465 the accuracy of the traditional linear regression (Table 2 and Fig. 5), and the results  
466 were better than those obtained with B1-B6 reflectances as input variables (Fig. S1). As



467 a type of supervised machine learning algorithm, linear regression can be used to obtain  
468 certain learning criteria as expressions ( $y=w_0+w_1\times x_1+\dots+w_p\times x_p$ ) about the optimal  $w_i$   
469 solution. However, for complex targeted tasks, the fitting ability of linear regression is  
470 limited, and it cannot represent the real situation well. For example, a support vector  
471 machine can map data to another space, which can use a linear regression to distinguish  
472 the categories well. In complex environments (real world in machine learning), such as  
473 our large-scale database collected from different lakes (Fig. 1), there are various  
474 environmental factors as well as different seasons within a lake, that have an impact on  
475 the trophic parameters and optical characteristics of lakes. Likewise, we found that the  
476 enhanced input variables, like the band ratios, if appropriately corrected for the *TSI*,  
477 resulted in a better performance (Fig. S1). This is consistent with some applications of  
478 machine learning algorithms (Cao et al., 2020), in which the performance of machine  
479 learning was reduced when covariances of input features were incorporated. This allows  
480 us to find more interesting *TSI*-correlated band ratios for MSI imagery in machine  
481 learning.

482 Several machine learning algorithms generally have different advantages and  
483 applicability owing to their different main principles (Cao et al., 2020; Li et al., 2021).  
484 This can be found in our results of the validation exercise, which showed that XGBoost  
485 provided stable *TSI* estimates, with a slope close to 1 and a good fitting coefficient of  
486 the measured and derived values ( $R^2=0.87$ , slope=0.85, MAE= 3.15, RMSE=4.11) (Fig.  
487 4). Similarly, we can also find an excellent performance ( $R^2=0.85$ , slope=0.84,  
488 MAE=3.31, RMSE=4.34) for estimating *TSI* values by the random forest algorithm.  
489 This was likely because it is a summation of all weak learners, weighted by the native  
490 log odds of error. In the case of boosting, we make decision trees into weak learners by  
491 allowing every tree to make only one decision before prediction. In some cases,



492 XGBoost outperformed random forest. In addition, the support vector machine  
493 performed worse than XGBoost and random forest (Fig. 4). Li et al. (2021) used a  
494 support vector machine to estimate Chl-a concentrations with a relatively small dataset  
495 of 32 samples and 273 samples, respectively. This is consistent with the recent process  
496 in the development of support vector machines and has many advantages for remote  
497 sensing applications with a small number of training datasets. Overall, the remote  
498 sensing and machine learning-based *TSI* model aims to reduce the dependence of  
499 traditional field measurements, while also providing a cost-effective approach to rapidly  
500 quantify the trophic state.

#### 501 **4.2 *TSI* model for lake classifications**

502 We validated the XGBoost *TSI* model considering different scenarios of lake  
503 classification, for example, water quality, optical absorption contributions, and  
504 reflectance spectra (Figs. 2 and 6). The results indicate three application scenarios for  
505 our model with low errors. The first one is of the XGBoost *TSI* model, which in  
506 particular, performed well (slope>0.91,  $R^2>0.91$ ) in high DOC (>3.88 mg L<sup>-1</sup>) and EC  
507 (>1000 μS cm<sup>-1</sup>) lakes (Fig. 6). We found that lakes with high EC level correspondingly  
508 showed a high DOC level (Table 1), for example, high average EC value of 5156.02 μS  
509 cm<sup>-1</sup> and high average DOC value of 18.75 mg L<sup>-1</sup> for NAP-type lakes. These brackish  
510 or saline lakes were distributed in the Tibet-Qinghai Plateau Region (e.g., KLK20, TS21,  
511 QHH22, SLC32, BMC34, ZRNMC36, NMC37) and Inner Mongolia-Xinjiang Plateau  
512 Limnetic Region (e.g., DL8, HSH10, DH17, HL18, WLSH16) (Table S1). Our results  
513 are in agreement with those of previous studies that DOC and EC of inland waters  
514 located in semi-arid region can be attributed to the evapo-concentration and  
515 accumulation processes (Curtis and Adams, 1995) as well as anthropogenic activities.  
516 Further, it can be observed that oligotrophic lakes accounting for 11.1% were also



517 distributed in the Tibet-Qinghai (Fig. 4).

518 Secondly, we found that our XGBoost *TSI* model performed well if the trophic  
519 parameters that correlated to the  $TSI_M(\text{Chl-a})$  or  $TSI_M(\text{SDD})$  dominated the lake  
520 classifications. Specifically, the high Chl-a (averaged  $14.26 \mu\text{g L}^{-1}$ ) and  $a_{ph}(440)$   
521 (averaged  $0.26 \text{ m}^{-1}$ ) levels in NAP-type lakes showed the best performance (slope=0.98,  
522  $R^2=0.88$ ) than those of other optical absorption contribution classifications (Fig. 6). In  
523 fact, there was a negligible difference in the performance for application in Phy-type  
524 and NAP-type lakes. For the third scenario, for the reflectance spectra classification,  
525 cluster-1 lakes with low TSM (averaged  $5.76 \text{ mg L}^{-1}$ ), turbidity (averaged 4.46 NTU),  
526 and  $a_d(440)$  (averaged  $0.26 \text{ m}^{-1}$ ) level, and high SDD level (average 2.38 m) also  
527 showed good performance (slope=0.91,  $R^2=0.87$ ) (Fig. 6). In general, *TSI*, as a  
528 comprehensive index incorporating the optical properties of itself, was calculated using  
529 trophic state parameters [ $TSI_M(\text{Chl-a})$ ,  $TSI_M(\text{SDD})$ , and  $TSI_M(\text{TP})$  in Eq. 7]. Our  
530 XGBoost *TSI* model performed best in the present study, which confirmed that the  
531 performance was mostly determined by biogeochemical environments in larger-scale  
532 regions. We cannot explain the dependence of the *TSI* model on the physico-optical  
533 properties. From another point of view, it can be inferred that the XGBoost *TSI* model  
534 applications mostly correlated to the Chl-a and SDD because of their high weight  
535 allocation in *TSI* equation.

536

### 537 **4.3 Trophic status in five limnetic regions**

538 According to this study more than 50% of lakes were eutrophic, indicating a  
539 long-standing status of eutrophication (Fig. 4), as seen by the mapping of 555 lakes by  
540 our XGBoost *TSI* model (Fig. 7). Some lake investigations undertaken earlier in China  
541 during 1978–1980 concluded that 41.2% lakes of eutrophication in China (Jin, 2003),



542 during 1988-1992 demonstrated that 51.2% lakes (Wang & Dou, 1998), during  
543 2001-2005 indicated that 84.5% lakes, during 2011-2019 showed that 50% lakes (Wen  
544 et al., 2019) were eutrophic or undergoing eutrophication. In our study, some historical  
545 records of Chl-a, SDD and TP from in comparison to earlier national investigation by  
546 Wang and Dou (1998) were collected in typical lakes, e.g., Dongting Lake, Poyang  
547 Lake, Chaohu Lake, Taihu Lake and Jingpo Lake, respectively (Table S5). Evidently,  
548 Chinese lakes have deteriorated considerably in terms of water quality at an alarming  
549 rate for typical lakes, e.g., Jingpo Lake, Dongting Lake and Poyang Lake, during past  
550 ~22 years (Table S5). Lake eutrophication is influenced by both natural (hydrological  
551 processes, topography, lake depth, and buffer capacity) factors as well as anthropogenic  
552 factors (land-use changes, urbanization construction, and domestic and industrial  
553 pollution) (Müller et al., 1998). A large-scale overview of lake eutrophication indicated  
554 there was a significant difference (ANOVA,  $F=255.2$ ,  $p<0.001$ ) in the five limnetic  
555 regions (Wang & Dou 1998). Owing to the imbalanced development of economic  
556 (Fig.S2, GDP and population), geological topography (Fig.S3, solar radiation intensity  
557 and sunshine hours) and climate (Fig.S4, annual temperature and precipitation), it was  
558 not surprising that the eutrophic lakes were generally distributed in the Eastern Plain  
559 Limnetic Region and Northeast Plain Limnetic Region, as well as that the oligotrophic  
560 lakes were found in the Tibet-Qinghai Plateau Limnetic Region (Fig.4 and Fig.7).

561 Considering the natural factors for the distributions of Chinese lake eutrophication,  
562 we could suppose some possibility that lake depth and lake hydrological processes  
563 cause the eutrophication of lakes in China. Previous studies (Wang & Dou 1998; Huang  
564 et al., 2014) have demonstrated that lakes with mean depths  $> 5$  m in China are mainly  
565 located in the Yungui Plateau Limnetic Region, Inner Mongolia-Xinjiang Plateau  
566 Limnetic Region, and Tibet-Qinghai Plateau Limnetic Region, whereas almost all lakes



567 located in the Eastern Plain Limnetic Region are shallow. Both these lakes in the  
568 Eastern Plain Limnetic Region are hydraulically connected with the Yangtze River with  
569 a temporary residence time of approximately 30 days (Fig. S7). In shallow lakes, due to  
570 wind waves or disturbance by fishes, the phosphorus/nitrogen nutrients stored in the  
571 sediment can be easily resuspended and released into the overlying water (Niemistö et  
572 al., 2008). Consequently, an increased frequency of algal blooms can be found in  
573 Eastern Plain Limnetic Region, in lakes, such as Taihu, Chaohu, and Hongze (Qin et al.,  
574 2019; Yao et al., 2016). Instead, deeper lakes, such as the ones in YGPLR and TQPLR,  
575 possess relatively good buffer capacity for waste-water runoff (Huang et al., 2014).  
576 Carvalho et al. (2009) found that Chl-a levels decreased with lake water depth and  
577 geographic location. Qin et al. (2020) and Tong et al., (2006) demonstrated that  
578 phosphorus reduction can mitigate eutrophication in deep lakes, and more efforts to  
579 reduce both N and P need to be undertaken in shallow lakes. This can be demonstrated  
580 in our case of Fuxian Lake with changeable eutrophication levels, with an average depth  
581 of 87 m, which was the deepest lake in southwest China (Fig. S7). In addition, the  
582 annual precipitation and air temperatures were relatively high in the EPLR (Fig. S4).  
583 Hydrological and meteorological processes can scour land surfaces and bring nutrients  
584 into lakes via rivers. Therefore, lake ecosystems were strongly related to the lake basin  
585 morphology and its hydrologic characteristics, which were higher in shallow lakes than  
586 in deep ones (Köiv et al., 2011).

587 On the other hand, human-induced eutrophication, for example, agricultural  
588 fertilization (Carpenter, 2008; Huang et al., 2017), aquaculture (Guo & Li, 2003) and  
589 sewage discharge (Paerl et al., 2011), are increasing terrestrial nutrient phosphorus but  
590 not nitrogen concentration inputs (Schindler et al., 2008). We suspected that two  
591 interactive factors, such as land-use and nutrient variations cause lake eutrophication,



592 because this can be found in our investigation of distributed lakes in the EPLR in  
593 comparison to earlier national investigation by Wang and Dou (1998). Many lakes in the  
594 EPLR that were naturally connected with rivers have been modified to paddy fields, and  
595 some small lakes have become isolated for lake aquaculture. For instance, Lake  
596 Dongting was artificially shifted from being river-fed to dammed/isolated. Logically it  
597 should a dam can settle down the suspended matter and nutrients via river inputs. But  
598 the shallow characteristic and wind mixing influence process significantly increased the  
599 probability of eutrophication (Liu et al., 2019). In EPLR and NPLR, 94% of China's  
600 population lives in 43% of its eastern region, which visually demonstrates the  
601 distribution of GDP with a densely populated east (Fig. S2). Owing to the requirements  
602 of water source utilization, the EPLR has lost one-third of its original lake areas to  
603 cropland since 1949 (Yin and Li, 2001). Lake aquaculture is highly active in these areas.  
604 These processes could lead to terrestrial nutrient loading into lakes, from either  
605 agriculture or aquaculture, and thereby alter the trophic state levels of a lake ecosystem.  
606 In 2019, the total fish catch was 4,695,432, 25,588,135, 2,314,603, and 4,841,159 tons  
607 in Hubei, Jiangxi, Anhui, and Jiangsu in the east, respectively (China rural statistical  
608 yearbook).

609       Although we have not systematically analyzed the effects of environmental factors  
610 on trophic status, some of the sparse existing comparative literature supported certain  
611 spatiotemporal patterns. It should be emphasized that China has been facing serious lake  
612 eutrophication and unbalanced distributions. Almost invariably, lake ecosystem health  
613 would still be impacted by stresses integrating anthropogenic and overexploitation of  
614 catchment resources. Consequently, addressing the issue of worsening eutrophication  
615 requires a better understanding of the environmental interactive mechanisms in the  
616 future.



## 617 **5 Conclusions**

618 Our study presents a novel remote sensing- and machine-learning-based algorithm  
619 applied in that allow to retrieve the lake TSI from Sentinel-2 MSI imagery. We used a  
620 match-up database ( $N=431$ ) over a diverse range of bio-optical regimes to train machine  
621 learning algorithms and validated it against the in situ data. The trophic states of 555  
622 lakes were then evaluated. These results provide a better understanding how remote  
623 sensing and machine learning-based models allow to estimate eutrophication over a  
624 large scale of different lakes. Our main findings can be summarized as follows:

625 1) Linear regression enabled us to find certain band combinations sensitive to *TSI*  
626 ( $R^2>0.59$ ), for example, the blue/red [ $Rrs(443)/Rrs(740)$ ,  $Rrs(492)/Rrs(740)$ ] and  
627 green/red [ $Rrs(560)/Rrs(704)$ ,  $Rrs(665)/Rrs(704)$ ] band ratios.

628 2) XGBoost algorithm resulted in optimum performance with  $R^2=0.87$  and  
629 slope=0.85, considering the low errors (MAE=3.15, RMSE=4.11), compared to the  
630 support vector machine and random forest algorithms.

631 3) If there is some preliminary data available from the study area one can improve  
632 the performance of the machine learning by dividing the lakes based on high DOC/EC,  
633 NAP-type and Phy-type, and cluster-1 reflectance spectra.

634 4) The trophic states of 555 lakes were evaluated in five limnetic regions;  
635 eutrophic lakes dominated in Eastern Plain Limnetic Region and Northeast Plain  
636 Limnetic Region, and most lakes in Tibet-Qinghai Plateau Limnetic Region were  
637 mesotrophic or oligotrophic.

638 In our subsequent research and management, qualification and mapping of *TSI* will  
639 be implemented as a remote sensing and machine learning model in a large-scale study,  
640 allowing for an improved performance. In the future, Sentinel-2 MSI data could be used  
641 to reveal spatiotemporal variations in lake trophic states in long-term time-series





642 responding to climate and anthropogenic activities.

643

#### 644 **CRedit authorship contribution statement**

645 Sijia Li: Conceptualization, Methodology, Formal analysis, Visualization, Funding  
646 acquisition, Writing original draft. Kaishan Song: Resources, Supervision, Project  
647 administration, Funding acquisition, Writing-review & editing. Tiit Kuster:  
648 Writing-review & editing. Ge Liu: Resources, Writing-review & editing. Shiqi Xu:  
649 Methodology. Zhidan Wen: Resources, Writing-review & editing. Yingxin Shang:  
650 Resources, Writing-review & editing. Lili Lyu: Investigation & Resources. Hui Tao:  
651 Investigation & Resources.

652

#### 653 **Acknowledgements**

654 The research was jointly supported by the China postdoctoral science foundation  
655 (2020M681056), the “Young support talents program” from Science and Technology  
656 Association of Jilin Province (2020-2023) to Dr. Sijia Li (QT202017), the National  
657 Natural Science Foundation of China (4217011915) and the Environmental Protection  
658 Project of Jilin Provincial Ecology and Environment Department (Nos. 2020-18). The  
659 authors thank all staff and students for their persistent assistance with both field  
660 sampling and laboratory analysis.

661

#### 662 **References**

663 APHA, A. W., Standard Methods for the examination of water and wastewater 20th  
664 edition.,<https://doi.org/10.2105/AJPH.51.6.940-a,1961>.  
665 American Public Health Association/American Water Works Association/Water Environment



- 666 Federation, Washington DC, USA,<https://doi.org/10.1080/23267224.1919.10651076>,1998.
- 667 Aizaki, M., Otsuki, A., Fukushima, T., et al., Application of Carlson's trophic state index to Japanese  
668 lakes and relationships between the index and other parameters: With 2 figures and 4 tables in the  
669 text. Internationale Vereinigung für theoretische und angewandte Limnologie: Verhandlungen, 21(1),  
670 675-681.[Res.rep.natl.inst.environ.stud.jpn](https://doi.org/10.1080/23267224.1919.10651076), 1981.
- 671 Carpenter, S. R., Brock, W. A., Cole, J. J., et al., Leading indicators of trophic cascades. *Ecol. Lett.*  
672 11(2), 128-138,<https://doi.org/10.1111/j.1461-0248.2007.01131.x>,2008.
- 673 Carlson, R. E., A trophic state index for lakes 1. *Limnol. Oceanogr.* 22(2),  
674 361-369.<https://doi.org/10.2307/2834910>,1977.
- 675 Cleveland, J. S., Weidemann, A. D., Quantifying absorption by aquatic particles: A multiple  
676 scattering correction for glass-fiber filters. *Limnol. Oceanogr.* 38(6), 1321-1327,  
677 <https://doi.org/10.4319/lo.1993.38.6.1321>,1993.
- 678 Cunha, D. G. F., do Carmo Calijuri, M., Lamparelli, M. C., A trophic state index for  
679 tropical/subtropical reservoirs (TSItsr). *Ecol. Eng.* 60, 126-134.  
680 <https://doi.org/10.1016/j.ecoleng.2013.07.058>,2013.
- 681 Curtis, P. J., Adams, H. E., Dissolved organic matter quantity and quality from freshwater and  
682 saltwater lakes in east-central Alberta. *Biogeochemistry* 30(1), 59-76.  
683 <https://doi.org/10.1007/bf02181040>,1995.
- 684 Doerffer, R., Schiller, H., The MERIS Case 2 water algorithm. *Int. J Remote sens.* 28(3-4), 517-535.  
685 <https://doi.org/10.1080/01431160600821127>,2007.
- 686 Duarte, C. M., Prairie, Y. T., Montes, C., et al., CO<sub>2</sub> emissions from saline lakes: A global estimate  
687 of a surprisingly large flux. *J. Geophys. Res.-Biogeosciences* 113(G4).  
688 <https://doi.org/10.1029/2007jg000637>,2008.
- 689 Drusch, M., Del Bello, U., Carlier, S., et al., Sentinel-2: ESA's optical high-resolution mission for



- 690 GMES operational services. Remote Sens. Environ. 120, 25-36,  
691 <https://doi.org/10.1109/igarss.2007.4423394>, 2012.
- 692 Fragoso Jr, C. R., Marques, D. M. M., Ferreira, T. F., et al., 2011. Potential effects of climate change  
693 and eutrophication on a large subtropical shallow lake. Environ. Modell. Softw. 26(11), 1337-1348,  
694 <https://doi.org/10.1016/j.envsoft.2011.05.004>, 2011.
- 695 Gitelson, A. The peak near 700 nm on radiance spectra of algae and water: relationships of its  
696 magnitude and position with chlorophyll concentration. International Journal of Remote Sensing,  
697 13(17), 3367-3373, <https://doi.org/10.1080/01431169208904125>, 1992.
- 698 Gitelson, A. A., Dall'Olmo, G., Moses, W., et al., 2008. A simple semi-analytical model for remote  
699 estimation of chlorophyll-a in turbid waters: Validation. Remote Sens. Environ. 112(9), 3582-3593.  
700 <https://doi.org/10.1080/01431169208904125>, 1992.
- 701 Gurlin, D., Gitelson, A. A., Moses, W. J., Remote estimation of chl-a concentration in turbid  
702 productive waters—Return to a simple two-band NIR-red model?. Remote Sens. Environ. 115(12),  
703 3479-3490. <https://doi.org/10.1016/j.rse.2011.08.011>, 2011.
- 704 Guo, L., Li, Z., Effects of nitrogen and phosphorus from fish cage-culture on the communities of a  
705 shallow lake in middle Yangtze River basin of China. Aquaculture 226(1-4), 201-212.  
706 [https://doi.org/10.1016/S0044-8486\(03\)00478-2](https://doi.org/10.1016/S0044-8486(03)00478-2), 2003.
- 707 Huang, C., Wang, X., Yang, H., et al., Satellite data regarding the eutrophication response to human  
708 activities in the plateau lake Dianchi in China from 1974 to 2009. Sci. Total Environ. 485, 1-11.  
709 <https://doi.org/10.1016/j.scitotenv.2014.03.031>, 2014.
- 710 Huang, J., Xu, C. C., Ridoutt, B. G., et al., Nitrogen and phosphorus losses and eutrophication  
711 potential associated with fertilizer application to cropland in China. J. Clean. Prod. 159, 171-179.  
712 <https://doi.org/10.1016/j.jclepro.2017.05.008>, 2017.
- 713 Hu, M., Zhang, Y., Ma, R., et al., Optimized remote sensing estimation of the lake algal biomass by



714 considering the vertically heterogeneous chlorophyll distribution: Study case in Lake Chaohu of  
715 China. *Sci. Total Environ.* 771, 144811. <https://doi.org/10.1016/j.scitotenv.2020.144811>,2021.

716 ILEC/Lake Biwa Research Institute 1994 1988-1993 survey of the state of the world's lakes Volumes  
717 I-IV (International Lake Environment Committee, Otsu and United Nations Environment  
718 Programme: Nairobi, Kenya)

719 Jeffrey, S. T., Humphrey, G. F., New spectrophotometric equations for determining chlorophylls a, b,  
720 c1 and c2 in higher plants, algae and natural phytoplankton. *Biochemie und physiologie der pflanzen*  
721 167(2), 191-194. [https://doi.org/10.1016/0022-2860\(75\)85046-0](https://doi.org/10.1016/0022-2860(75)85046-0),1975.

722 Jin, X., Hu, X., A comprehensive plan for treating the major polluted regions of Lake Taihu, China.  
723 *Lakes & Reservoirs: Research & Management* 8(3-4), 217-230.  
724 <https://doi.org/10.1111/j.1440-1770.2003.00220.x>,2003.

725 Jin, X., Xu, Q., Huang, C., Current status and future tendency of lake eutrophication in China.  
726 *Science in China Series C: Life Sciences* 48(2), 948-954.<https://doi.org/10.1007/BF03187133>,2005.

727 Kloiber, S. M., Brezonik, P. L., Olmanson, L. G., et al., A procedure for regional lake water clarity  
728 assessment using Landsat multispectral data. *Remote Sens. Environ.* 82(1), 38-47.  
729 [https://doi.org/10.1016/S0034-4257\(02\)00022-6](https://doi.org/10.1016/S0034-4257(02)00022-6),2002.

730 Koiv, T., Nõges, T., Laas, A., Phosphorus retention as a function of external loading, hydraulic  
731 turnover time, area and relative depth in 54 lakes and reservoirs. *Hydrobiologia* 660(1), 105-115.  
732 <https://doi.org/10.1007/s10750-010-0411-8>,2011.

733 Li, S., Song, K., Wang, S., et al., Quantification of chlorophyll-a in typical lakes across China using  
734 Sentinel-2 MSI imagery with machine learning algorithm. *Sci. Total Environ.* 778, 146271.  
735 <https://doi.org/10.1016/j.scitotenv.2021.146271>,2021.

736 Liu, D., Duan, H., Yu, S., et al., 2019. Human-induced eutrophication dominates the bio-optical  
737 compositions of suspended particles in shallow lakes: Implications for remote sensing. *Sci. Total*



- 738 Environ. 667, 112-123. <https://doi.org/10.1016/j.scitotenv.2019.02.366>
- 739 Lund, J. W., Eutrophication. *Nature* 214(5088), 557-558. <https://doi.org/10.1038/214557a0,1967>.
- 740 Ma, Y. L., Zhang, W. B., Yu, B., et al., Prevalence of allergic bronchopulmonary aspergillosis in  
741 Chinese patients with bronchial asthma. *Zhonghua jie he he hu xi za zhi= Zhonghua jiehe he huxi*  
742 *zazhi= Chinese journal of tuberculosis and respiratory diseases*, 34(12), 909-913.  
743 <https://doi.org/10.1038/cmi.2011.4,2011>.
- 744 Matthews, M. W., Eutrophication and cyanobacterial blooms in South African inland waters: 10  
745 years of MERIS observations. *Remote Sens. Environ.* 155, 161-177.  
746 <https://doi.org/10.1016/j.rse.2010.04.013,2014>.
- 747 Matthews, M. W., Odermatt, D., Improved algorithm for routine monitoring of cyanobacteria and  
748 eutrophication in inland and near-coastal waters. *Remote Sens. Environ.* 156, 374-382.  
749 <https://doi.org/10.1016/j.rse.2014.10.010,2015>.
- 750 Mortsch, L. D., Quinn, F. H., Climate change scenarios for Great Lakes Basin ecosystem studies.  
751 *Limnol. Oceanogr.* 41(5), 903-911. <https://doi.org/10.4319/lo.1996.41.5.0903,1996>.
- 752 Morel, A., Prieur, L., 1977. Analysis of variations in ocean color 1. *Limnol. Oceanogr.* 22(4),  
753 709-722.
- 754 Müller, B., Lotter, A. F., Sturm, M., et al., Influence of catchment quality and altitude on the water  
755 and sediment composition of 68 small lakes in Central Europe. *Aquat. Sci.* 60(4), 316-337.  
756 <https://doi.org/10.1007/s000270050044,1998>.
- 757 Mountrakis, G., Im, J., Ogole, C., Support vector machines in remote sensing: A review. *ISPRS-J.*  
758 *Photogramm. Remote Sens.* 66(3), 247-259. <https://doi.org/10.1016/j.isprsjprs.2010.11.001,2011>.
- 759 Neil, C., Spyrakos, E., Hunter, P. D., et al., A global approach for chlorophyll-a retrieval across  
760 optically complex inland waters based on optical water types. *Remote Sens. Environ.* 229, 159-178.  
761 <https://doi.org/10.1016/j.rse.2019.04.027,2019>.



- 762 Niemistö, J., Holmroos, H., Pekcan-Hekim, Z., et al., Interactions between sediment resuspension  
763 and sediment quality decrease the TN: TP ratio in a shallow lake. *Limnol. Oceanogr.* 53(6),  
764 2407-2415. <https://doi.org/10.2307/40058331>,2008.
- 765 OECD (Organization for Economic Cooperation and Development). 1982. Eutrophication of waters:  
766 monitoring, assessment and control. Organisation for Economic and Cooperative Development,  
767 Paris, France.
- 768 Oliver, S. K., Collins, S. M., Soranno, P. A., et al., Unexpected stasis in a changing world: Lake  
769 nutrient and chlorophyll trends since 1990. *Glob. Change Biol.* 23(12), 5455-5467 .  
770 <https://doi.org/10.1111/gcb.13810>,2017.
- 771 Olmanson, L. G., Bauer, M. E., Brezonik, P. L., A 20-year Landsat water clarity census of  
772 Minnesota's 10,000 lakes. *Remote Sens. Environ.* 112(11), 4086-4097.  
773 <https://doi.org/10.1111/jawr.12138>,2008.
- 774 Pan, Q., Dias, D., An efficient reliability method combining adaptive support vector machine and  
775 Monte Carlo simulation. *Struct. Saf.* 67, 85-95. <https://doi.org/10.1016/j.strusafe.2017.04.006>,2017.
- 776 Paerl, H., Nutrient and other environmental controls of harmful cyanobacterial blooms along the  
777 freshwater–marine continuum. In *Cyanobacterial harmful algal blooms: State of the science and*  
778 *research needs* (pp. 217-237). Springer, New York, NY.  
779 [https://doi.org/10.1007/978-0-387-75865-7\\_10](https://doi.org/10.1007/978-0-387-75865-7_10),2008.
- 780 Paerl, H. W., Xu, H., McCarthy, M. J., et al., Controlling harmful cyanobacterial blooms in a  
781 hyper-eutrophic lake (Lake Taihu, China): the need for a dual nutrient (N & P) management strategy.  
782 *Water Res.* 45(5), 1973-1983. <https://doi.org/10.1016/j.waters.2010.09.018>,2011.
- 783 Pahlevan, N., Chittimalli, S. K., Balasubramanian, S. V., et al., Sentinel-2/Landsat-8 product  
784 consistency and implications for monitoring aquatic systems. *Remote Sens. Environ.* 220, 19-29.  
785 <https://doi.org/10.1016/j.rse.2018.10.027>,2019.



786 Pahlevan, N., Smith, B., Schalles, J., et al., Seamless retrievals of chlorophyll-a from Sentinel-2 (MSI)  
787 and Sentinel-3 (OLCI) in inland and coastal waters: A machine-learning approach. *Remote Sens.*  
788 *Environ.* 240, 111604. <https://doi.org/10.1016/j.rse.2019.111604>, 2020.

789 Prieur, L., Sathyendranath, S., An optical classification of coastal and oceanic waters based on the  
790 specific spectral absorption curves of phytoplankton pigments, dissolved organic matter, and other  
791 particulate materials 1. *Limnol. Oceanogr.* 26(4), 671-689.  
792 <https://doi.org/10.4319/lo.1981.26.4.0671>, 1981.

793 Qin, B., Gao, G., Zhu, G., et al., Lake eutrophication and its ecosystem response. *Chinese Sci. Bull.*  
794 58(9), 961-970. <https://doi.org/10.1007/s11434-012-5560-x>, 2013.

795 Qin, B., Zhou, J., Elser, J. J., et al., Water depth underpins the relative roles and fates of nitrogen and  
796 phosphorus in lakes. *Environ. Sci. Technol.* 54(6), 3191-3198.  
797 <https://doi.org/10.1021/acs.est.9b05858>, 2020.

798 Quayle, W. C., Peck, L. S., Peat, H., et al., Extreme responses to climate change in Antarctic lakes.  
799 (Climate Change). *Science* 295(5555), 645-646. <https://doi.org/10.1126/science.1064074>, 2002.

800 Reichstein, M., Camps-Valls, G., Stevens, B., et al., Deep learning and process understanding for  
801 data-driven Earth system science. *Nature* 566(7743), 195-204.  
802 <https://doi.org/10.1038/s41586-019-0912-1>, 2019.

803 Rodhe, W., 1969. Crystallization of eutrophication concepts in northern Europe.

804 Sass, G. Z., Creed, I. F., Bayley, S. E. et al., Understanding variation in trophic status of lakes on the  
805 Boreal Plain: A 20 year retrospective using Landsat TM imagery. *Remote Sens. Environ.* 109(2),  
806 127-141. <https://doi.org/10.1016/j.rse.2006.12.010>, 2007.

807 Schindler, D. W., Hecky, R. E., Findlay, D. L., et al., Eutrophication of lakes cannot be controlled by  
808 reducing nitrogen input: results of a 37-year whole-ecosystem experiment. *Proceedings of the*  
809 *National Academy of Sciences*, 105(32), 11254-11258.



- 810 <https://doi.org/10.1109/ICASSP.2002.5745032>,2008.
- 811 Sheela, A. M., Letha, J., Joseph, S., et al.,Trophic state index of a lake system using IRS (P6-LISS
- 812 III) satellite imagery. Environ. Monit. Assess. 177(1), 575-592.
- 813 <https://doi.org/10.1007/s10661-010-1658-2>,2011.
- 814 Shi, K., Zhang, Y., Song, K., et al., 2019. A semi-analytical approach for remote sensing of trophic
- 815 state in inland waters: Bio-optical mechanism and application. Remote Sens. Environ. 232, 111349.
- 816 Smith, V. H., Tilman, G. D., Nekola, J. C.,Eutrophication: impacts of excess nutrient inputs on
- 817 freshwater, marine, and terrestrial ecosystems. Environ. Pollut. 100(1-3), 179-196.
- 818 <https://doi.org/10.1016/j.rse.2019.111349>,1999.
- 819 Smith, V. H., Joye, S. B., Howarth, R. W., 2006. Eutrophication of freshwater and marine
- 820 ecosystems. Limnol. Oceanogr. 51(1part2), 351-355.
- 821 [https://doi.org/10.4319/lo.2006.51.1\\_part\\_2.0351](https://doi.org/10.4319/lo.2006.51.1_part_2.0351),2006.
- 822 Smith, V. H., Schindler, D. W.,Eutrophication science: where do we go from here?. Trends Ecol.
- 823 Evol. NLM. 24(4), 201-207. <https://doi.org/10.1016/j.tree.2008.11.009>,2009.
- 824 Song, K., Li, L., Tedesco, L. P., et al.,Hyperspectral determination of eutrophication for a water
- 825 supply source via genetic algorithm–partial least squares (GA–PLS) modeling. Sci. Total Environ.
- 826 426, 220-232. <https://doi.org/10.1016/j.scitotenv.2012.03.058>,2012.
- 827 Song, K. S., Zang, S. Y., Zhao, Y., et al.,Spatiotemporal characterization of dissolved carbon for
- 828 inland waters in semi-humid/semi-arid region, China. Hydrol. Earth Syst. Sci. 17(10).
- 829 <https://doi.org/10.5194/hessd-10-6559-2013>,2013a.
- 830 Song, K., Li, L., Tedesco, L. P., Li, S., 2013b. Remote estimation of chlorophyll-a in turbid inland
- 831 waters: Three-band model versus GA-PLS model. Remote Sens. Environ. 136, 342-357.
- 832 <https://doi.org/10.1016/j.rse.2013.05.017>,2013b.
- 833 Song, K., Liu, G., Wang, Q., et al.,Quantification of lake clarity in China using Landsat OLI imagery





- 834 data. *Remote Sens. Environ.* 243, 111800. <https://doi.org/10.1016/j.rse.2020.111800>,2020.
- 835 Thiemann, S., Kaufmann, H., 2000. Determination of chlorophyll content and trophic state of lakes  
836 using field spectrometer and IRS-1C satellite data in the Mecklenburg Lake District, Germany.  
837 *Remote Sens. Environ.* 73(2), 227-235. [https://doi.org/10.1016/S0034-4257\(00\)00097-3](https://doi.org/10.1016/S0034-4257(00)00097-3),2000.
- 838 Toming, K., Kotta, J., Uemaa, E., Sobek, S., Kutser, T., & Tranvik, L. J. Predicting lake dissolved  
839 organic carbon at a global scale. *Scientific reports* 10(1), 1-8.  
840 <https://doi.org/10.1038/s41598-020-65010-3>,2020.
- 841 Tong, Y., Zhang, W., Wang, X., et al.,Decline in Chinese lake phosphorus concentration  
842 accompanied by shift in sources since 2006. *Nature Geoscience*, 10(7), 507-511.  
843 <https://doi.org/10.1038/ngeo2967>,2017.
- 844 Tranvik, L. J., Downing, J. A., Cotner, J. B., et al.,Lakes and reservoirs as regulators of carbon  
845 cycling and climate. *Limnol. Oceanogr.* 54(6part2), 2298-2314.  
846 [https://doi.org/10.4319/lo.2009.54.6\\_part\\_2](https://doi.org/10.4319/lo.2009.54.6_part_2).2298,2009.
- 847 USEPA, A., 2002. National water quality inventory 2000 report. EPA-841-R-02-001.
- 848 Wetzel, R. G.,Limnology: lake and river ecosystems. gulf professional publishing.  
849 <https://doi.org/10.1086/380040>,2001.
- 850 Wang, S., Li, J., Zhang, B., et al.,Trophic state assessment of global inland waters using a  
851 MODIS-derived Forel-Ule index. *Remote Sens. Environ.* 217, 444-460.  
852 <https://doi.org/10.1016/j.rse.2018.08.026>,2018.
- 853 Wang, S. and Hongsheng, D., 1998. Chinese Lake Records, Beijing, Science Publishing (in  
854 Chinese).
- 855 Warren, M. A., Simis, S. G., Martinez-Vicente, et al.,Assessment of atmospheric correction  
856 algorithms for the Sentinel-2A MultiSpectral Imager over coastal and inland waters. *Remote Sens.*  
857 *Environ.* 225, 267-289. <https://doi.org/10.1016/j.rse.2019.03.018>,2019.



- 858 Wen, Z., Song, K., Liu, G., et al., Quantifying the trophic status of lakes using total light absorption  
859 of optically active components. *Environ. Pollut.* 245, 684-693.  
860 <https://doi.org/10.1016/j.envpol.2018.11.058>,2019.
- 861 Wiley, C., What motivates employees according to over 40 years of motivation surveys. *International*  
862 *journal of manpower.* <https://doi.org/10.1108/01437729710169373>,1997.
- 863 Wu, G., Xu, Z., Prediction of algal blooming using EFDC model: Case study in the Daoxiang Lake.  
864 *Ecol Modell.* 222(6), 1245-1252. <https://doi.org/10.1016/j.ecolmodel.2010.12.021>,2011.
- 865 Yao, Y., Wang, P., Wang, C., et al., Assessment of mobilization of labile phosphorus and iron across  
866 sediment-water interface in a shallow lake (Hongze) based on in situ high-resolution measurement.  
867 *Environ. Pollut.* 219, 873-882. <https://doi.org/10.1016/j.envpol.2016.08.054>,2016.
- 868 Yin, H., Li, C., Human impact on floods and flood disasters on the Yangtze River. *Geomorphology*  
869 41(2-3), 105-109. [https://doi.org/10.1016/S0169-555X\(01\)00108-8](https://doi.org/10.1016/S0169-555X(01)00108-8),2001.
- 870 Yin, H., Douglas, G. B., Cai, Y., et al., Remediation of internal phosphorus loads with modified clays,  
871 influence of fluvial suspended particulate matter and response of the benthic macroinvertebrate  
872 community. *Sci. Total Environ.* 610, 101-110. <https://doi.org/10.1016/j.scitotenv.2017.07.243>,2018.
- 873 Zhang, Y., Zhou, Y., Shi, K., et al., Optical properties and composition changes in chromophoric  
874 dissolved organic matter along trophic gradients: Implications for monitoring and assessing lake  
875 eutrophication. *Water Res.* 131, 255-263. <https://doi.org/10.1016/j.watres.2017.12.051>,2018.